Optimizing performance and operational stability of CsPbI$_3$ quantum-dots based light emitting diodes by interface engineering

K. M. Muhammed Salim,[1] Ehsan Hassanabadi,[1] Sofia Masi,[1] Andrés. F. Gualdrón-Reyes,[1] Marius Franckevicius,[2] Andrius Devižis,[2] Vidmantas Gulbinas,[2] Azhar Fakharuddin,[3,4,5] Iván Mora-Seró[*1]*

[1] Institute of Advanced Materials (INAM), University Jaume I, Avenida de Vicent Sos Baynat, s/n, 12071 Castelló de la Plana, Castellón, Spain

[2] Center for Physical Sciences and Technology, Sauletekio av. 3, LT-10257 Vilnius, Lithuania

[3] IMEC, Kapeldreef 75, 3001 Leuven, Belgium

[4] Department of Electrical Engineering, KU Leuven, Kasteelpark Arenberg, 3001 Leuven, Belgium

[5] Department of Physics, University of Konstanz. D-78464, Germany

Abstract

Perovskite light-emitting diodes (PeLEDs) have emerged as a promising candidate for next-generation display technology and lighting applications owing to their high current efficiency, low operating voltage, narrow spectral emission and tuneable emission colour. Keys to achieving efficient PeLEDs are, beside an emitter layer with high optical quality, negligible charge injection barrier between charge injecting layers (CILs) and an optimized thickness of these CILs for a controlled flow of charge carriers through the device. In this study, we systematically optimized hole transport layers (HTL) and electron transport layers (ETL) in PeLEDs employing CsPbI$_3$ quantum dots (QDs) as an emitter layer. We also investigated two bilayer cathodes (Liq/Ag and LiF/Al) with the various ETLs employed in our study and observed that 2,4,6-tris[3-(diphenylphosphinyl)phenyl]-1,3,5-triazine (PO-T2T) as ETL improves the band alignment, leading to better electron injection. The improved electron/hole current balance results in ~63% higher external quantum efficiency (EQE) in PO-T2T based devices compared to PeLEDs employing other ETLs. In addition, we tracked the operational

stability of the different devices observing a correlation with the EQE, where samples with higher EQE (PO-T2T based devices) also present the highest stable operation at elevated current densities.

TOC
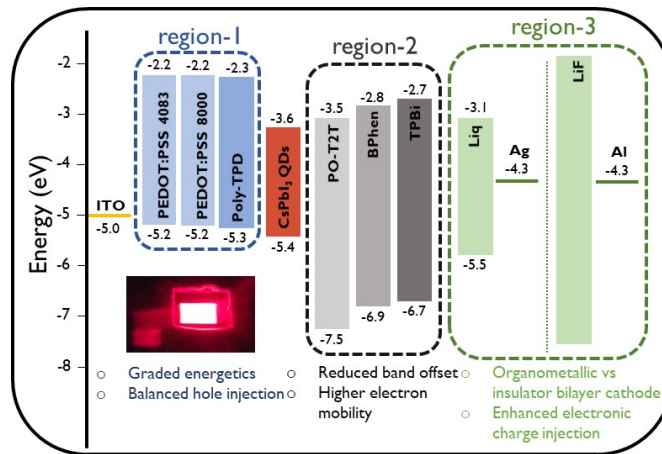
Introduction

Recently-emerging metal halide perovskites have led to breakthroughs in numerous optoelectronic devices such as solar cells, light emitting diodes (LEDs), optically-pumped lasers, photodetectors and others.[1-3] Their remarkable performance is attributed to their unique photophysical properties such as high photoluminescence quantum yield (PLQY), high defect tolerance, good charge-transport abilities and so on.[3-4] After initial success in photovoltaic devices, halide perovskites also gained considerable attention for use in LEDs.[3-5] The first working perovskite LED (PeLED) was reported in 2014 with a hybrid organic-inorganic $CH_3NH_3PbBr_3$ as an emitter layer. It showed an external quantum efficiency (EQE) of 0.1% and low device stability.[6] A subsequent surge in research activities to improve device performance and stability resulted in state-of-the-art external quantum efficiency (EQE) of over 21%, which is comparable with the well-established organic LEDs (OLEDs) and quantum dot LEDs (QLEDs) without additional light outcoupling.[7-9] The tremendous progress in PeLEDs was achieved by combining various material and device engineering aspects, for instance, by using quantum-confined perovskite nanocrystals,[10] by employing 2D/3D mixed perovskite systems with cascaded bandgaps that allow funnelling of charge carriers,[11-12] nanocrystal pinning by polymer encapsulation,[7] and surface passivation via additive engineering that led to over 70% PLQY in perovskite thin films[12].

Generally in LEDs, an imbalanced charge injection would cause electron or hole accumulation at device interfaces, and carrier leaks through the device without contributing to photon emission.[3, 5, 13-14] This fact reduces the EQE and wall plug efficiency (ratio between input power and output power of an LED).[13] For an efficient LED design, it is imperative to judiciously select hole and electron transport layers (HTL & ETL, respectively) to ensure the balanced charge injection and transport.[15-18] The carrier mobility in these layers is also

important to obtain a high wall plug efficiency. For example, Li et al demonstrated a significant improvement in EQE and current efficiency of PeLEDs when the hole mobility of HTL is matched well with electron mobility of ETL.[19] Recently, it is demonstrated that the characteristics (conductivity, energetics, etc.) of charge transport/injection layers are also crucial for EQE roll-off and operational stability of PeLEDs.[15] Lifetime of PeLEDs employing mixed 2D/3D perovskite emitter layers was tuned from several minutes to a few tens of hours by balancing charge injection into the emitter layer. Such a systematic study for PeLEDs employing inorganic nanocrystals or quantum dots (QDs) is desired to improve their performance and stability.

Another crucial but relatively underexplored aspect is to meliorate electron injection from cathodes to the ETL in standard stack LEDs (employing a HTL on a conducting substrate) and to balance it with the holes flowing through the device.[16, 20] Typical metal electrodes such as aluminium (Al), silver (Ag), or gold (Au) are the most commonly used.[12, 15, 21] The high work function of Al, Ag, and Au makes electron injection in low-voltage electroluminescence devices arduous.[22] To overcome this issue, thin buffer layers (also often reported as electron injection layer, EIL) are employed with the metal electrode (bilayer cathode) to reduce the cathode work function.[23-24] Typical examples include inorganic alkali/alkaline metal/compounds LiF/Al[10, 12, 23] or LiF/Au,[21] Cs_2CO_3/Al,[18, 25] CsF/Al,[26] CaF/Al,[27] Ca/Al[28] or Ca/Ag;[29] organic alkali/alkaline metal complex 8-Quinolinolato lithium (Liq)/Al[24, 30] or Liq/Ag,[31] 8-Quinolinolato sodium (Naq)/Al,[32] Cesium quinoline-8-oxide (Csq)/Al[33] and so on. Although the precise mechanism behind the enhanced electron injection of bilayer cathode is still unknown, plausible explanations are related with the metal-induced chemical reduction of the EIL and the subsequent doping of the ETL layer, or by charge injection via quantum tunnelling.[21, 31, 34-38] It is important to note that Liq is a metal-organic semiconductor and LiF is an insulator, and therefore, a small change in LiF thickness could severely affect the

formation of band bending zone and restrict electron injection.[38-40] Therefore, an efficient LED operation also requires tuning of EIL/metal interface beside ETL/emitter or HTL/emitter interfaces. So far, no direct comparison of such bi-layers, for example, metal-organic complex Liq/Ag with insulator compound LiF/Al has been made, in terms of their charge-injection performance and corresponding EQE of LEDs.

In this work, we systematically investigated and optimized HTL/emitter and ETL/emitter interfaces in PeLEDs employing inorganic $CsPbI_3$ QDs as emitter layer, as well as single or double washing cycles of $CsPbI_3$ QDs. We investigated Poly(N,N'-bis-4-butylphenyl-N,N'-bisphenyl)benzidine (Poly-TPD) and Poly(3,4-ethylenedioxythiophene) polystyrene sulfonate (PEDOT:PSS; 4083 and 8000, with high and low conductivity, respectively) and also a bi-layer of the two as HTLs. PEDOT 8000/PTPD bilayer HTL showed highest EQE amongst all the HTLs employed, which we attributed to a controlled hole-injection due to its more resistive nature. To meliorate electron injection, the various ETLs investigated in this study are 2,4,6-tris[3-(diphenylphosphinyl)phenyl]-1,3,5-triazine (PO-T2T), Bathophenanthroline (BPhen), and 2,2',2''-(1,3,5-Benzinetriyl)-tris(1-phenyl-1-H-benzimidazole) (TPBi). To further tune electron injection, we compared the performance of two bilayer cathodes (Liq/Ag and LiF/Al) with all the ETLs) in $CsPbI_3$ QDs based PeLEDs. Amongst the three ETLs employed, PO-T2T based PeLEDs excels in performance and also show a higher stability at elevated current densities, with stable operation during 10 minutes while a degradation of the operational stability is observed for the rest of samples. It shows superior performance with Liq/Ag bilayer cathode (luminance of 3762 cd m^{-2} at ~8.7V and EQE of 6.2%) than LiF/Al bilayer counterpart (luminance of 1305 cd m^{-2} at ~9.3V and EQE of 3.8 %). A similar trend is observed for BPhen ETL whereas contrarily, TPBi ETL show a higher performance with LiF/Al cathode than its Liq/Ag counterpart. Through detailed

5

electrical characterization of PeLEDs, we explain these differences in performance and stability upon changing these various interfaces.

Results and Discussion

a) Morphological and optical properties of as-synthesized CsPbI$_3$ QDs

Inorganic CsPbI$_3$ QDs were synthesized via a hot injection method.[41-42] The detailed synthesis procedure is given in the experimental section. These QDs are subsequently washed to remove the excess capping organic ligands surrounding them. X-ray diffraction (XRD) pattern shows the typical (100) and (200) planes, indicating that the QDs crystallize in a simple cubic phase (Fig. S1a).[43-44] Transmission electron microscopy (TEM) images of single and double washed QDs (Figure 1) provide insights into their morphology. Statistical analysis performed over 280 single washed QDs (Fig. 1a, Fig. S2a and b) showed that QDs exhibit a size distribution around 9.77±2.32 nm (Fig. 1b), while the double washed QDs (Fig. 1c) showed a size distribution of 11.56±1.65 nm (calculated from 154 QDs in Fig 1d, Fig. S2c and d). The size of these QDs is in the range of excitonic Bohr radius values (8-12 nm),[43] and thus quantum confinements effects are expected to take place in these QDs. The second washing cycle decreases the size distribution and concomitantly increases the average size as a consequence of the extra centrifugation process and agglomeration effect.[19] The CsPbI$_3$ QDs showed an absorption onset at 660 nm and a narrow photoluminescence (PL) emission centred at 676 nm (with FWHM ~40 nm), as shown in Fig. S1b. Moreover, the single washed QDs showed a PLQY of ~92% (and double washed QDs with 75-80%), and a PL decay lifetime of ~25 ns, see Fig. S1c.
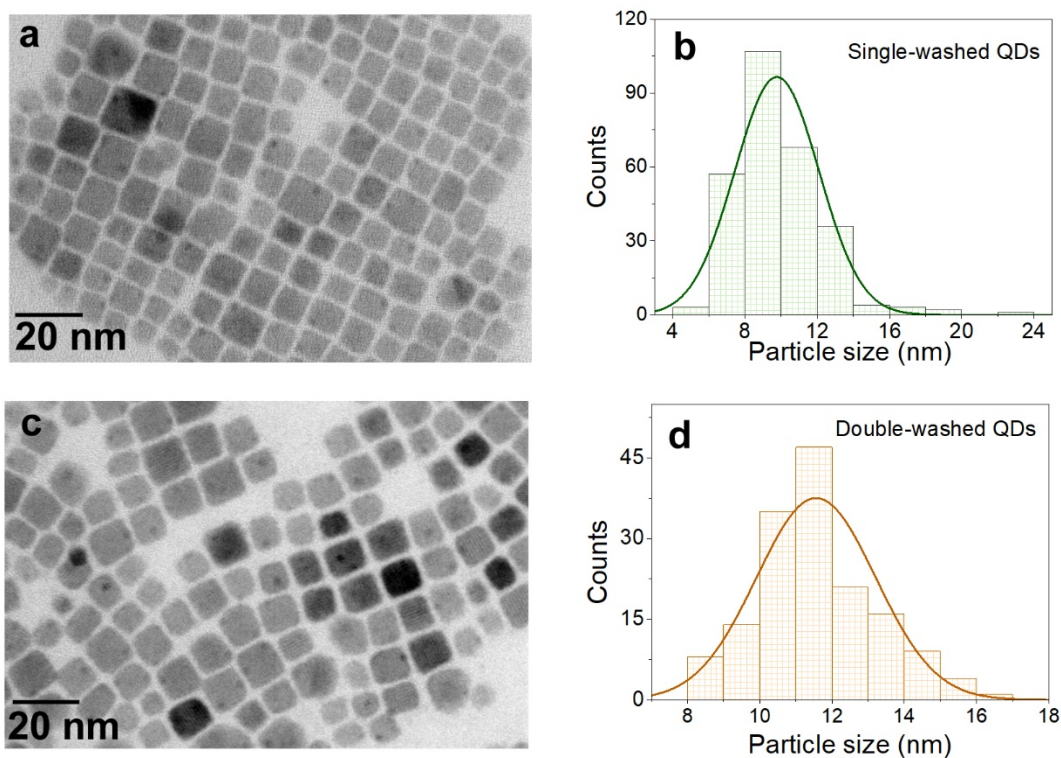
Figure 1: Transmission electron microscopy images and particle size distribution of (a and b) single-washed and (c and d) double-washed CsPbI$_3$ QDs. The size distribution of the QDs, was calculated from over 150 QDs of each type. The images used to calculate size distribution are provided in Fig. S2a-d.

Prior to using these QDs as an emitter layer in LEDs, we investigated their photophysical properties using time-resolved photoluminescence (PL) and transient absorption spectroscopy (TAS). Steady-state PL spectra of the QDs are shown in Fig. 2a. The double-washed QDs show a red-shifted PL emission peak centred at 670 nm as compared to those of single-washed QDs (664 nm), which can be attributed to their larger average size. The double washing reduces the density of capping ligands, thus resulting in clustering of these QDs during centrifuge process. The time-resolved transients of both the samples (Fig. 2b-d) show that the double-washed QDs have slightly faster PL decay, more apparent at longer time scales (Fig. 2d and Fig. S3) and slightly lower PL intensity than their single washed counterparts. Taking into account some variations between samples, the double washing reduces the PL yield by about (10-30)%. A decrease in PL intensity can be understood from the fact that the double-washing process reduces surface ligands density on the QDs, as surface ligands also act as

surface passivation agents.[45-46] This fact, consequently increases the density of non-radiative carrier recombination sites and hence reduces the PL features.[45, 47] The PL decay is not a single exponential and shows no clear dependence on excitation intensity (Fig. S3), indicating that the decay rate is governed by linear processes, i.e. the carrier trapping and geminate recombination. The obtained fitting parameters are provided in Table S1 and S2.

In order to gain further insights into the charge kinetics of the single and double washed QDs, we performed Transient Absorption Spectroscopy (TAS) measurements (Fig. 2e and f, Fig. S4 and S5). Both kinds of QDs show bleaching of ground state (GS) absorption at the absorption band edge at ~660 nm. Notably, the GS bleach show ~8 nm red shift for double washed QDs which matches closely with the shift in PL emission peak. Both the QDs show induced absorption bands located at around 700 nm, on the edge of stationary absorption. These bands are attributed to the hot-carrier cooling taking place on a hundreds of femtoseconds timescale (Fig. S4 & S5). We estimate one photon absorption in one QD corresponds to ~4 $\mu J \cdot cm^{-2}$. This corroborates our pump probe data (Fig. 2): at the lowest excitation intensity of 5.5 $\mu J \cdot cm^{-2}$, statistically two e-h pairs are created in a fraction of QDs. Their recombination causes a fast decay component observed during initial hundreds of ps, while at longer times, a single e-h pair recombines with the time constant of about 10 ns (Fig. 2d). At higher excitation intensities, the initial decay becomes faster due to recombination of several e-h pairs. Dependence of the luminescence intensity on the excitation intensity shows that the deviation from the linear growth starts by exceeding about 18 $\mu J \cdot cm^{-2}$ excitation intensity (Fig. 2f), thus also when statistically more than one e-h pair are created in some QDs. Consequently, it shows that carrier diffusion is strongly restricted within the single-washed nanocrystal. The restricted carrier motion is apparently an important factor determining high PL yield of the nanostructured perovskites; charge carriers cannot easily reach nonradiative recombination centres present only in some QDs. Slightly stronger PL saturation was observed for the double

8

washed samples (see inset in Fig. 2a) suggesting that carrier diffusion between nanocrystals is less restricted. This conclusion is also supported by the faster and more non-exponential PL and transient absorption decays in double-washed samples where, due to less restricted diffusion, carriers may reach non-radiative recombination centres present in neighbouring QDs or recombine non-geminately. More efficient carrier motion in double-washed samples is expected for QDs containing lower number of insulating ligands. The restricted carrier motion character may also additionally influence performance of PeLEDs by hampering carrier transport.
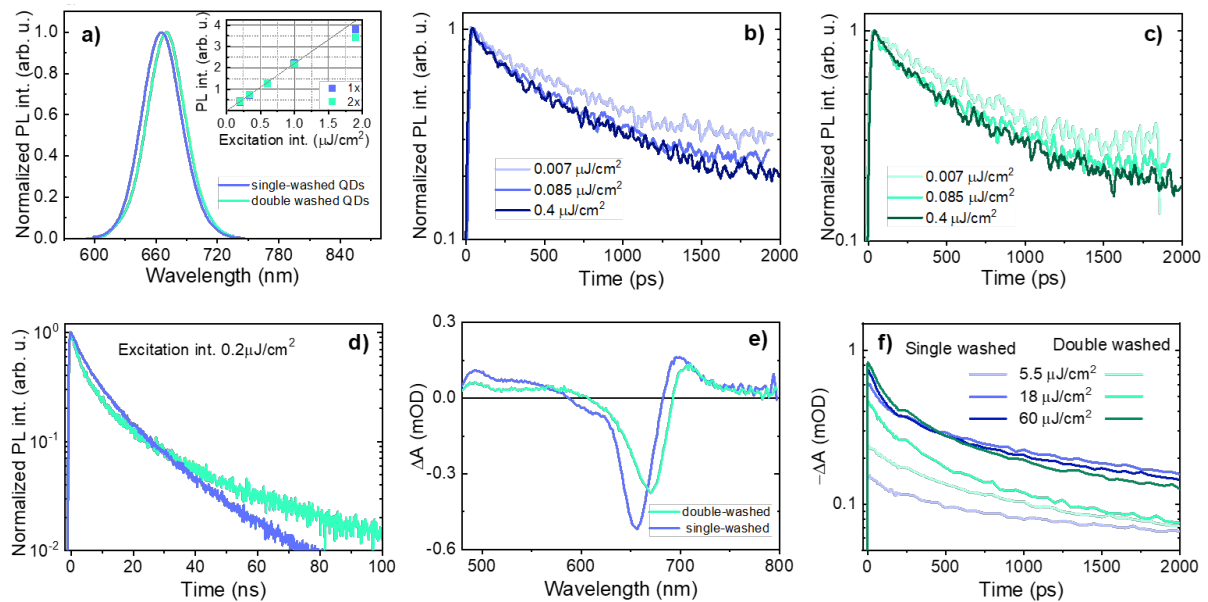

Figure 2: Steady-state photoluminescence (PL) spectra of once-washed and double-washed $CsPbI_3$ QDs (a). Inset in (a) shows PL intensity as a function of excitation energy density (values are extracted from Fig. S3) of the thin films made of the two types of QDs. Fig. (b) and (c) shows time-resolved PL lifetime of perovskite QDs measured with streak camera and (d) using TRSPC. (e) Transient absorption spectra of the both QD films at t = 1ps (energy density 18 $\mu J/cm^2$), and (f) presents transient absorption kinetics of the ~660 nm band at 5.5$\mu J/cm^2$ excitation energy.

b) Optimization of HTL/CsPbI₃ QD emitter interface to manipulate hole transport/injection

In order to understand the performance of these QDs in PeLEDs, we employed them as an emitter layer. At first, we optimized hole transport/injection in these devices (see Fig. 3 for the architecture, ITO/HTL/CsPbI₃ QDs/PO-T2T (40 nm)/Liq (2 nm)/Ag (100 nm)). Unless

stated otherwise, we used once-washed QDs throughout this study. For this study, PO-T2T was used as ETL and Liq was used as buffer layer (or electron injection layer, EIL). The various HTLs investigated are: PEDOT:PSS 4083, PEDOT:PSS 8000, and Poly-TPD and their optimized thickness is adapted based on the values reported in literature.[8, 12, 15-16, 28] We used both types of PEDOT:PSS in a bilayer HTL configuration as follows: (see Fig. 3, **region 1**): PEDOT:PSS 4083/Poly-TPD bilayer HTL (hereafter named as 4083/PTPD) and PEDOT:PSS 8000/Poly-TPD bilayer HTL (8000/PTPD) and compared its performance with a Poly-TPD single layer HTL (hereafter named as PTPD). The key difference between the two types of PEDOT:PSS layers is that the PEDOT:PSS 8000 is PSS enriched and has a lower hole conductivity (10^{-5}-10^{-6} S cm^{-1}) than PEDOT:PSS 4083 (10^{-3}-10^{-4} S cm^{-1}).[16, 48]
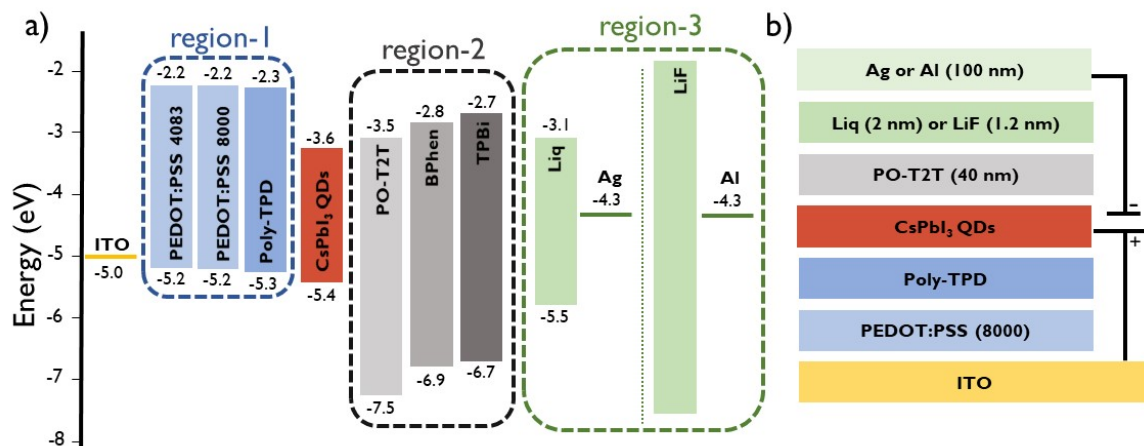

Figure 3: Energy levels diagram of various HTLs, ETLs, and bilayer cathodes employed in this study. a) In of the first step of HTL optimization, PEDOT:PSS 4083, PEDOT:PSS 8000 and Poly-TPD (refer region-1) in a device stack of ITO/HTL/CsPbI$_3$ QDs/PO-T2T (40 nm)/Liq (2 nm)/Ag (100 nm) were investigated. Subsequently, In the case of bilayer cathode (refer region-3) optimization with various ETLs, (refer region-2, PO-T2T, BPhen, TPBi), we employed two sets of PeLED configurations (Type-1 and Type-2). The Type-1 device with a configuration of ITO/(8000/PTPD)/CsPbI$_3$ QDs/(PO-T2T, BPhen, TPBi) (40 nm)/Liq (2 nm)/Ag (100 nm) and Type-2 device with a configuration of ITO/(8000/PTPD)/CsPbI$_3$ QDs/(PO-T2T, BPhen, TPBi) (40 nm)/LiF (1.2 nm)/Al (100 nm). b) The configuration of the champion device using a bilayer cathode (Liq/Ag and LiF/Al) together with optimized CILs.

Current density-voltage-luminance (J-V-L) curves of PTPD based devices (Fig. S6a) show a turn-on voltage (V_{ON}) of 4.90 V, which is higher than its bilayer counterparts. The V_{ON} for 8000/PTPD and 4083/PTPD devices were 3.30 V and 4.10 V, respectively (see Table S3

for a summary of device performance values). The higher V_{ON} in the case of PTPD devices suggests ineffective hole injection and higher voltage losses at the HTL/perovskite interface, which improves when PEDOT:PSS based bilayer HTL is employed. The 8000/PTPD based devices show higher luminance and EQE (both champion and average, see Fig. 4) than their 4083/PTPD counterparts despite nearly an order of magnitude lower current passing through them (Fig. S6a). The difference in performance between the two types of PEDOT:PSS based PeLEDs is due to their different conductivity: PEDOT:PSS 8000 is more insulating in nature due to higher PSS contents (PEDOT:PSS ratio 1:20) than PEDOT:PSS 4083 (PEDOT:PSS ratio 1:6).[16] Since the electron transport/injection remain unchanged in both devices (both devices employ the same ETL), we attribute the superior performance of 8000/PTPD devices to a more balanced electron/hole currents as compared to 4083/PTPD devices. The excess current in the case of the latter leaks through the device without contributing to radiative recombination, and therefore, leads to a lower EQE/luminance. Not only PEDOT:PSS 8000 regulates hole injection into the emitter layer,[16] its more insulating surface can also inhibit exciton quenching at the interface which explains the higher EQE in PeLEDs employing it. A statistical analysis of over ten devices of each type further confirms that the 8000/PTPD based LEDs show a higher average and champion EQE (5.3 and 6.2%, respectively), followed by 4083/PTD devices (2.3 and 4.3%, respectively), as shown in Fig. 4a. PeLEDs employing PTPD alone as HTL showed the lowest average and champion EQE (0.6 and 2.3%, respectively) and the highest performance variation measured over 13 devices.

Our assumption of more balanced charge injection in the case of 8000/PTPD bilayer HTL is confirmed by the EL spectra of the three devices at a fixed current density, $J = 4$ mA/cm^2 (Fig. 5a). A significantly enhanced EL intensity in 8000/PTPD PeLED compared to other devices affirms that most injected charge carriers contribute to light emission (highest current efficiency) in these devices. Very notably, the PeLEDs employing 8000/PTPD HTL

showed significantly enhanced stability at constant J (Fig. 4b), with a stable performance during 10 minutes in contrast with the other devices where a performance decrease is observed during this period. This fact further suggests the beneficial role of balanced charge injection in achieving operational stability.[15] The 8000/PTPD devices showed only 10% drop in the initial EQE after 10 min at a continuous biasing, whereas the 4083/PTPD and PTPD devices showed 74% and 50% drop within 7 and 2 min, respectively. The stability trends further confirm that a higher charge balance is achieved in 8000/PTPD devices. Moreover, Fig. S7 shows, the appearance of similar/narrow PL and EL (a representative PeLED from 8000/PTPD) spectra corroborate the material stability of $CsPbI_3$ QDs in the thin film of fabricated devices.
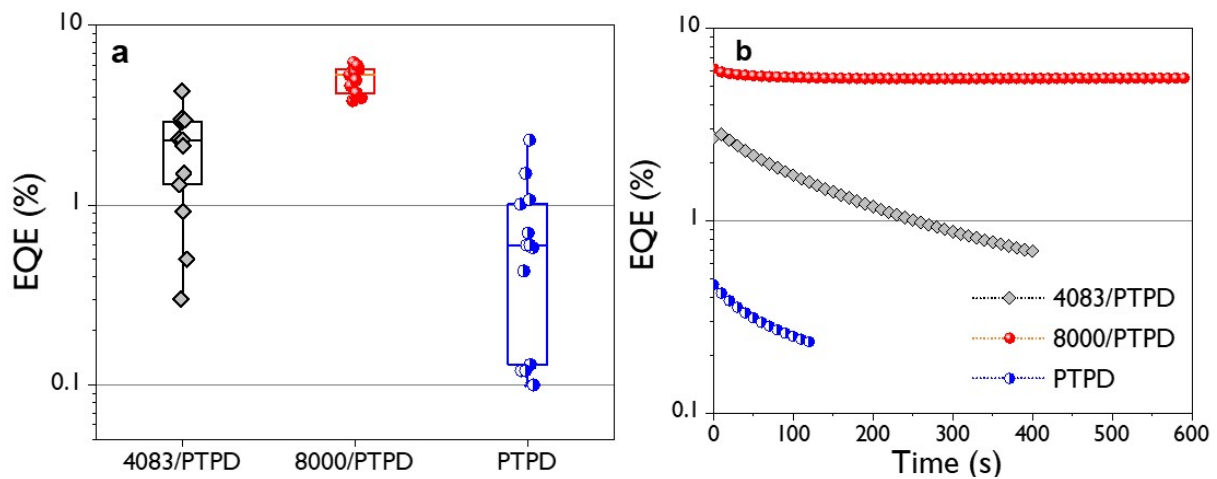

Figure 4: a) Statistical distribution of the EQE of 4083/PTPD, 8000/PTPD, and PTPD HTL based devices (ITO/HTL/CsPbI$_3$QDs/PO-T2T/Liq/Ag) . Individual data points are taken from 13 devices of each type. b) Operational stability of representative devices of each type at $J = 4$ mA/cm^2.

c) Manipulating surface ligand density of the CsPbI$_3$ QDs

We note a higher V_{ON} in our all PeLEDs. The best-performing 8000/PTPD PeLEDs demonstrate $V_{ON} = 3.30$ V, which is nearly twice the photon energy of CsPbI$_3$ QDs emission.[44] A plausible explanation is that the CsPbI$_3$ QDs are capped with long-chain insulating organic ligands that hinder charge carrier transport/injection into the QDs emitter layer. We carried out

an additional washing cycle (double-washing) to remove excess capping ligands surrounding these CsPbI$_3$ QDs and employed them as an emitter layer in our optimized device architecture (ITO/(8000/PTPD)/CsPbI$_3$ QDs/PO-T2T (40 nm)/Liq (2 nm)/Ag (100 nm)). We observed a significant decrease of V$_{ON}$ when double-washed QDs are used as active layer in PeLEDs, showed a V$_{ON}$ of 2.25 V see Fig. S6c, confirming the excess of ligand as one of the responsible for high V$_{ON}$ observed in PeLEDs using single-washed QDs. However, double-washed QDs PeLED showed significantly lower performance than their single-washed counterparts, see Fig. S6d and Table S4).
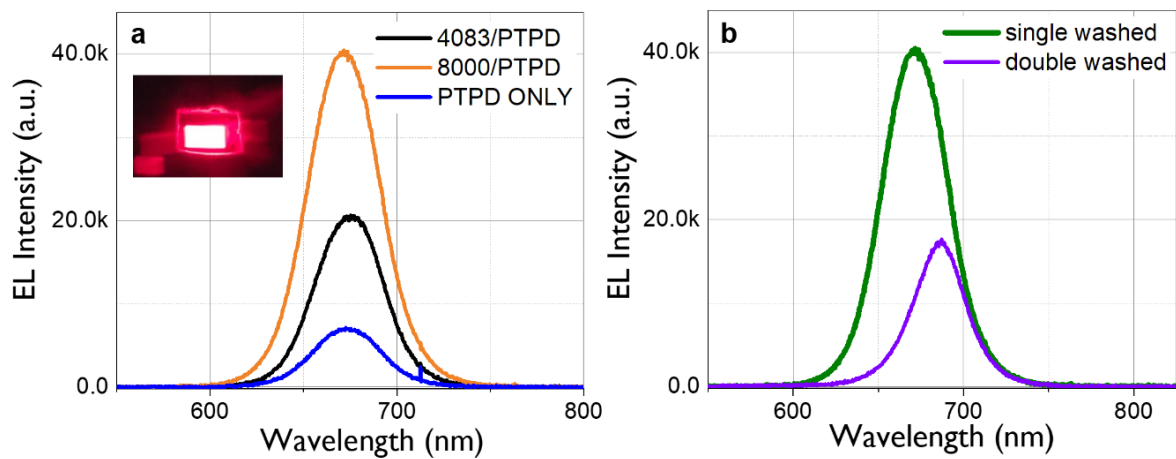
Figure 5: (a) Electroluminescence (EL) spectra of PeLEDs employing three different HTLs measured at 4 mA/cm^{-2}. The device architecture is ITO/HTL/CsPbI$_3$ QDs/PO-T2T (40 nm)/Liq (2 nm)/Ag (100 nm. Inset shows a photograph of 8000/PTPD based PeLED at 4 mA/cm^2, (b) EL spectra of PeLEDs employing single and double washed QDs at 4 mA/cm^2.

The deleterious effects of the additional washing cycle on QDs morphology is further evident from the EL spectra (Fig. 5b). At a given $J = 4$ mA/cm^2, the EL intensity of the double washed QDs PeLED drops to nearly half compared to its single washed counterpart. A factor that influences the reduction of EL is the lower PLQY observed for double-washed QDs, as it was discussed. However, PLQY alone does not explain the observed drop in EQE of PeLEDs. Probably, faster carrier transport is also detrimental for the PeLED performance since charge carriers in the CsPbI$_3$ EML do not have enough time to recombine during the short transit though the perovskite layer, which ultimately find non-radiative recombination pathways.

d) Optimization of electron transport and injection layers

In order to further understand the impact of various ETLs and EILs on PeLEDs performance, we fabricated two types of device architectures (see Fig. 3, region-2 and region-3). The key difference between these two architectures is the EIL, e.g., Liq/Ag or LiF/Al bilayer cathode. We investigated suitability of both architectures with three ETLs, namely, PO-T2T, BPhen, and TPBi while keeping the HTL unchanged (8000/PTPD).

Figure 6a shows EQE of PeLEDs employing three ETLs with device configurations ITO/(8000/PTPD)/CsPbI$_3$ QDs/(PO-T2T, BPhen, TPBi) (40 nm)/Liq (2 nm)/Ag (100 nm). Clearly, the PO-T2T based devices results in the highest EQE (both average and champion) as compared to the BPhen and TPBi counterparts. J-V-L spectra and EQE curves are shown in Fig. S10 and the device performance parameters are shown in Table S6. We attribute the higher performance in PO-T2T devices to a better energy level alignment of PO-T2T with CsPbI$_3$ QDs and its higher conductivity as compared to the other two ETLs. The flat band energy level of PO-T2T (-3.5 eV) matches well with the conduction band (CB) of CsPbI$_3$ QDs (-3.6 eV), which reduces losses at ETL/perovskite interface.[28] In addition, PO-T2T has a higher electron mobility ($\approx10^{-3}$ cm^2.V^{-1}.s^{-1})[28] than BPhen (3.9×10^{-4} cm^2 V^{-1} s^{-1}),[15, 18] and TPBi (3.3×10^{-5} cm^2 V^{-1} s^{-1}),[18] that favours more efficient electron transport. The more favourable energetics and higher mobility of PO-T2T also explain the lower V$_{ON}$ in PO-T2T based devices. An added benefit of PO-T2T is its improved hole blocking properties due to its lower-lying HOMO (-7.5 eV) level (Fig. 3, region-2). Contrarily, BPhen and TPBi ETLs provide a higher offset for charge injection (0.8 and 0.9 eV, respectively) and inferior electron mobility compared to PO-T2T, which lead to a higher V$_{ON}$, lower EQE (Fig. 6a and Fig. S11), and lower luminance (see Fig. S10). Furthermore, we studied the PO-T2T ETL thickness (30, 40, and 50 nm) to probe any effect on charge injection/transport properties. The J-V-L spectra (see Fig. S8, Fig S9 and

14

Table S5) show nearly identical V_{ON} for all, however, the current density, luminance and EQE in these devices largely differ.

Not only do PO-T2T PeLEDs show a higher initial EQE, but also a more stable performance at continuous biasing. Fig. 6b shows that PO-T2T PeLED retains ~90% of its initial EQE after 10 min of continuous biasing at 4 mA/cm^2, whereas BPhen and TPBi counterparts only retained 13% and 51% of their initial EQE even when biased for a shorted time (~4 min). Similarly, Fig. S12a shows the comparative stability (EQE vs time plot) of PO-T2T/Liq/Ag device at various current density values (1, 4, 8, 16, 40, 80, and 160 mA/cm^2). It can be observed that, the optimised device can retain the stability at relatively lower current density scans, and it started to deplete at higher current density which could be associated with the material stability and charge imbalance (at 80 and 160 mA/cm^2 scans). Moreover, Fig. S12b and c show the, EQE vs time and corresponding EL emission wavelength vs time spectra of a best performed device (PO-T2T/Liq/Ag) at 1 mA/cm^2 scan. A stable EL emission during the course of current scan is observed.
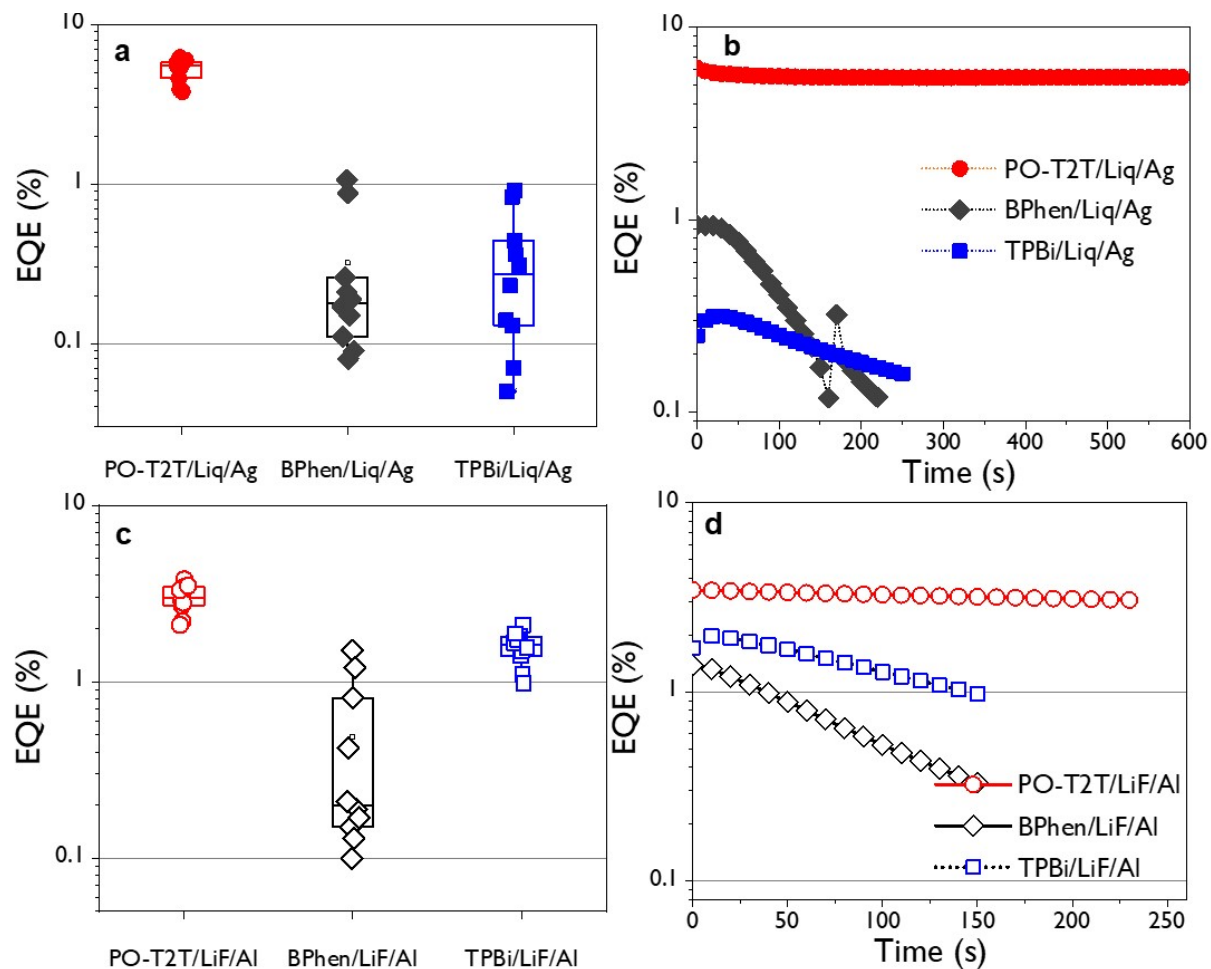
Figure 6: a) Statistical distribution of the EQE of PeLEDs employing three different ETLs, namely, PO-T2T, BPhen, and TPBi devices with Liq/Ag for bilayer cathode optimization study. Individual data points are taken from 10 devices of each types. b) Stability of representative devices of each type in (a), measured at a constant current density (4 mA/cm^2). (c) and (d) show the EQE statistics and stability, respectively, of the same three ETLs with LiF/Al bilayer cathode.

In the case of LiF/Al cathode, the initial EQE of all three ETLs based PeLEDs is lower than their Liq/Ag counterparts, see Fig. 6c and Fig. S11. Once again, PO-T2T leads to the highest EQE of 3.8%, but its performance is lower than the Liq/Ag analogues (EQE 6.2%). Interestingly, TPBi and BPhen based PeLEDs showed higher EQE of 2.1% and 1.5% with LiF/Al cathode as compared with Liq/Ag counterpart (EQE of 0.91 & 1.1%), respectively. Also, the average as well as the best EQE for TPBi is higher when LiF/Al cathode is used, suggesting a better energy level alignment. For the PO-T2T and BPhen, Liq/Ag cathode layer offers a better energy level alignment for charge injection. These assumptions are validated by

the device operation at continuous biasing at 4 mA/cm^2, see Fig. 6d. The PO-T2T device shows the highest stability followed by TPBi (similar to their EQE trends) and BPhen PeLED showed the least stable performance with LiF/Al cathode. This is a slightly different trend compared to the Liq/Ag cathode, where the least efficient and least stable devices were those made of TPBi. In addition, Fig. S13a shows the comparative stability (EQE vs time plot) of PO-T2T/LiF/Al device at various current density values (1, 4, 8, 16, 40, 80, and 160 mA/cm^2). We also noticed that, the optimised device can retain the stability at relatively lower current density scans, and it started to deplete at higher current density scans (at 80 and 160 mA/cm^2 scans, similar to the behaviour observed for the PO-T2T/Liq/Ag device). Moreover, Fig. S13b and c show the, EQE vs time and corresponding EL emission wavelength vs time spectra of a device at 1 mA/cm^2 scan, demonstrating the stable EL emission during the progression of current scan. These results clearly indicated that efficient and stable PeLEDs require a careful optimization of all the device heterostructures.

Conclusions

In summary, we investigated the role of various HTLs (single and bilayer), ETLs, electron injection layer (EIL, or buffer layer), emitter layers (associated with the washing cycles of emitting QDs), as well as cathode layer on current efficiency, turn-on voltage, EQE, and operational stability in CsPbI$_3$ quantum-dot perovskite light emitting diodes (PeLEDs). Regarding HTL optimization, we note that a bilayer HTL configuration leads to higher performance than a single layer HTL as it probably forms a graded interface favouring charge injection. We also noted that HTL with a lower conductivity (PEDOT:PSS 8000) leads to a higher EQE. We attribute this to a more controlled hole flow and suppression of exciton quenching at the HTL/emitter interface.

Towards $CsPbI_3$ quantum dots (QDs) based emitter layer, we note crucial role of surface ligand density towards controlling optical quality of the films as well as device performance. We observed that multiple washing cycles negatively affect EQE and brightness, especially at elevated current density (J), regardless a reduction of the turn-on potential is observed, as consequence of the lower amount of long chain capping ligands on the QDs surface. An additional washing cycle although slightly reduces photoluminescence efficiency, however, much less than the drop in EQE of PeLEDs.

For controlling the electron transport/injection into the emitter layer, we varied the ETL thickness, and investigated three different ETLs (that differ in conductivity and energetic offset with respect to emitter layer). We note that a more favourable electron injection, together with an improved conductivity, leads to a higher EQE, a smaller EQE roll-off and a significantly higher operational stability at continuous biasing, linking balanced electron and hole currents not just with higher performance but with higher stability. Our optimized PeLEDs show an EQE of 6.2%, luminance of 3762 cd.m^{-2} at around 8.7 V (~25 mA/cm^2) a significantly smaller turn on voltage and also more stable operation at elevated current densities than un-optimized devices.

Experimental Section

Materials and chemicals:

All chemicals were purchased from Sigma Aldrich and used without purification unless stated otherwise. Cesium carbonate (Cs_2CO_3, 99.9%), lead (II) iodide (PbI_2, 99.9985%, TCI), oleic acid (OA, technical grade 90%), oleylamine (OAm, technical grade 70%), 1-octadecene (ODE, technical grade 90%), hexane (reagent grade ≥95%), octane (anhydrous, ≥99%), methyl acetate (MeOAc, anhydrous 99.5%). 2,4,6-Tris[3-(diphenylphosphinyl)phenyl]-1,3,5-triazine (PO-T2T, Lumtec Taiwan), 4,7-Diphenyl-1,10-phenanthroline (BPhen, Lumtec Taiwan),

18

2,2',2"-(1,3,5-Benzinetriyl)-tris(1-phenyl-1-H-benzimidazole) (TPBi, e-Ray Optoelectronics Technology), 8-Quinolinolato lithium (Liq, Ossila), and Poly-TPD (1-Materials).

Synthesis and purification of CsPbI$_3$ QDs:

CsPbI$_3$ QDs were synthesized according to the previous reports[42, 44, 49] with some modifications.[41] Briefly, 0.814g Cs$_2$CO$_3$, 2.5 mL (OA) and 40 mL of 1-ODE were mixed in a three-neck flask at 120 °C under vacuum for 60 min, keeping a constant stirring. Temperature of the mixture was increased to 150 °C under N$_2$-purge until the complete dissolution of Cs$_2$CO$_3$. Next, the temperature of resultant solution was decreased to 100 °C in order to avoid the Cs-oleate oxidation (Cs-oleate is one of the precursors used for injection).

In a typical CsPbI$_3$ QDs synthesis, 0.5 g of PbI$_2$ and 25 mL of 1-octadecene were degassed in a 100 mL three-neck flask at 120 °C for 1 h. Then 2.5 mL of both preheated (OA) and 2.5 mL of (OAm) were added under N$_2$ atmosphere to the mixture reaction. Here, halide precursor became transparent. Then the synthesis temperature was rapidly increased to 170 °C and 2 ml of preheated Cs-Oleate was quickly injected. After 5 sec, the reaction was quenched by immersing the three-neck flask in ice bath.

The purification of CsPbI$_3$ QDs was conducted by washing with anhydrous MeOAc. For single-washed QDs, 7.5 mL of crude solution and 17.5 mL of anhydrous MeOAc were centrifuged at 7500 rpm for 5 min. Then the supernatant was discarded, and the precipitate was recovered. The solid was re-dispersed in 7.5 mL of anhydrous hexane. For double-washed QDs, the QDs dispersion was centrifuged again with 4 mL anhydrous MeOAc for another 5 min. The supernatant was discarded and the solid was re-dispersed in 7.5 mL of anhydrous hexane. The solution of CsPbI$_3$ QDs were stored at least 24 hours in refrigerator (5 °C) prior to use (in order to precipitate excess of Cs-oleate and Pb-oleate).

Device Fabrication:

Devices were fabricated on pre-patterned ITO substrates. The substrates were cleaned with Extran soap water, distilled water, acetone, and IPA via sonication (15 min each). Subsequently, the substrates were dried with N_2 and exposed to oxygen plasma (200 W) for 10 min prior to the deposition of hole transporting layer (HTL). PEDOT:PSS used as HTL (Clevios 4083 and Clevios 8000; filtered with 0.45 μm PVDF filter). HTL was then spin coated for 30 s at 3,000 rpm and thermally annealed at 140 °C for 10 min. The substrates were stored in a nitrogen-filled glovebox for the spin coating of Poly-TPD layer. Poly-TPD (6 mg mL^{-1} in chlorobenzene) was spin coated on ITO substrates (1,000 rpm for 45s: acc. 6,000 rpm) and annealed at 140 °C for 10 min to form a bilayer HTL. The poly-TPD films were exposed to O_2 plasma (1–2 s at 100 W) to improve wetting properties. The CsPbI$_3$ QDs solution in octane (10 mg mL^{-1}) was deposited with a single step process at 3,000 rpm for 30 s and dried at room temperature. Subsequently, a 40 nm thick ETL (PO-T2T, BPhen, TPBi) was deposited via thermal evaporation (pressure $< 2 \times 10^{-6}$ mbar). The Liq (2 nm) and LiF (1.2 nm) were evaporated to form an electron injection layer. Ag and Al (100 nm) were used as metal back contact (cathode) that defined the active area of the devices (0.125 cm^2).

X-ray Diffraction (XRD) pattern characterization and transmission electron microscopy

The X-ray Diffraction (XRD) pattern of the thin film was recorded using an X-ray diffractometer (D8 Advance, Bruker AXS) (Cu Kα, wavelength of $\lambda = 1.5406$ Å) within the range of 10–60°.

UV-Vis Absorption spectra (UV-Vis), Photoluminescence Spectra (PL), Time Resolved Photoluminescence (TRPL) Decay profile

The steady state absorption spectra of CsPbI$_3$ QD solution was measured by using a UV/Vis absorption spectrophotometer (Varian, Cary 300). The emission measurement (PL spectra) and time resolved PL (TRPL) decay were collected by Horiba Fluorolog.

Transient Photoluminescence measurements

For the streak camera measurements, two femtosecond Yb:KGW lasers were employed. Yb:KGW oscillator (Light Conversion Ltd.) produced 80 fs, 1030 nm light pulses at a repetition rate of 76 MHz, which were frequency doubled to 515 nm (HIRO harmonics generator, Light Conversion Ltd.) and focused into an ≈30 μm spot on the sample. Excitation power was attenuated using neutral density filters. The maximum time resolution of the entire system was ≈13.0 ps.

Photoluminescence of the QDs films was measured using Edinburgh-F900 (Edinburgh Instruments) spectrometer. PL transients were obtained using Time-correlated single photon counting (TCSPC). The excitation source was a picosecond pulsed diode laser EPL-470 (Edinburgh Instruments) emitting ~100 ps pulses (2 MHz repetition frequency) with characteristic emission wavelength 470 nm.

Transient absorption spectroscopy of films

The transient absorption setup was based on the amplified femtosecond laser Pharos 10-600-PP laser (Light Conversion Ltd.), operating at fundamental wavelength of 1032 nm, repetition rate of 200 kHz and pulse width of <250 fs. The measurements were performed at repetition rate of 200/42=4.762 kHz frequency achieved by using the pulse picker. The collinear optical parametric amplifier Orpheus PO15F2L (Light Conversion Ltd.) was used to obtain 515 nm wavelength pulses for sample excitation. Excitation was modulated at 4.762/6=0.794 kHz frequency by mechanical chopper synchronized to the output of the pulse picker. As a probe, we used pulses, spectrally broadened by means of continuum generation in the sapphire crystal. The detection equipment consisted of Andor-Shamrock SR-500i-B1-R spectrometer (Andor Technology, 150 lines/mm diffraction grating) equipped with Andor-Newton (Andor Technology) DU970 CCD camera (1600 × 200 pixels). The reading of the camera was synchronized with the chopper.

Calculation of external quantum efficiency (EQE)

The EQE is calculated by counting number of photons generated the PeLED per second. This divided by number injected electrons/sec gives EQE.[15]

$$EQE = \frac{N_{photon}}{I_{inj}/q} X\ 100\%$$

Herein I_{inj} is the current injected (at a given applied bias V) into the LED, N_{photon} represents the number of photons per second, and q is elementary charge (1.6×10^{-19} C).

N_{photon} is calculated by

$$N_{photon} = \frac{I_{photo}}{hc} \frac{\int \lambda\, P^N(\lambda) d\lambda}{\int P^N(\lambda) R(\lambda) d\lambda}$$

Where I_{photon} is the photocurrent, measured by Newport 818-SL-L Silicon photodetector, $R(\lambda)$ is responsivity of the photodetector. Normalized power spectrum, $P^N(\lambda)$ is calculated as:

$$P^N(\lambda) = \frac{\frac{n(\lambda)hc}{\lambda}}{\int \frac{n(\lambda)hc}{\lambda}\, d\lambda} = \frac{n(\lambda)}{\lambda \int \frac{n(\lambda)}{\lambda d\lambda}}$$

where $n(\lambda)$ is the number of photons emitted at each wavelength, which is directly related to emission spectrum $S_{em}(\lambda)$. Thus, by normalizing both

$$\frac{n(\lambda)}{\int n(\lambda) d\lambda} = \frac{S_{em}(\lambda)}{\int S_{em}(\lambda) d\lambda}$$

$P^N(\lambda)$ is rewritten as

$$P^N(\lambda) = \frac{S_{em}(\lambda)}{\lambda \int \frac{S_{em}(\lambda)}{\lambda d\lambda}}$$

ASSOCIATED CONTENT

Supporting Information: Experimental section, XRD data, TEM images of $CsPbI_3$ QDs, UV-Vis spectra, PL Spectra, TRPL data, TAS studies. J-V-L curves (including the optimization of HTL, QD washings, ETL, and bilayer cathode studies), EQE vs current density plots (including the optimization of HTL, QD washing, ETL, and bilayer cathode studies),

AUTHOR INFORMATION

Corresponding Authors:

Email: sero@uji.es, azhar-fakhar.uddin@uni-konstanz.de

Author contributions

K.M.M.S. and E.H. contributed equally to this work. K.M.M.S., A.F. and I.M.S. conceived the idea and A.F. and I.M.S. oversaw the project. K.M.M.S. carried out device fabrication and characterization and wrote the first draft. E.H. synthesized quantum dots. S.M. and A.F.G.-R. helped and supervised QD preparation and characterization. M.F., A.D. and A.F. carried out photoluminescence and pump probe measurements. V.G. M.F and A.G. interpreted ultrafast measurements data. All the authors were involved in discussion on data analysis and contributed to manuscript preparation.

Notes

The authors declare no competing financial interest.

REFERENCES

1.   Jena, A. K.; Kulkarni, A.; Miyasaka, T., Halide Perovskite Photovoltaics: Background, Status, and Future Prospects. *Chem. Rev.* **2019,** *119* (5), 3036-3103.

2.   Quan, L. N.; Rand, B. P.; Friend, R. H.; Mhaisalkar, S. G.; Lee, T.-W.; Sargent, E. H., Perovskites for Next-Generation Optical Sources. *Chem. Rev.* **2019,** *119* (12), 7444-7477.

3.   Veldhuis, S. A.; Boix, P. P.; Yantara, N.; Li, M.; Sum, T. C.; Mathews, N.; Mhaisalkar, S. G., Perovskite Materials for Light-Emitting Diodes and Lasers. *Adv. Mater.* **2016,** *28* (32), 6804-6834..

4.   Fakharuddin, A.; Shabbir, U.; Qiu, W.; Iqbal, T.; Sultan, M.; Heremans, P.; Schmidt-Mende, L., Inorganic and Layered Perovskites for Optoelectronic Devices. *Adv. Mater.* **2019***, 31*, 1807095.

5.   Zou, Y.; Yuan, Z.; Bai, S.; Gao, F.; Sun, B., Recent progress toward perovskite light-emitting diodes with enhanced spectral and operational stability. *Mater. Today Nano* **2019,** *5*, 100028.

6.   Tan, Z.-K.; Moghaddam, R. S.; Lai, M. L.; Docampo, P.; Higler, R.; Deschler, F.; Price, M.; Sadhanala, A.; Pazos, L. M.; Credgington, D.; Hanusch, F.; Bein, T.; Snaith, H. J.; Friend, R. H., Bright light-emitting diodes based on organometal halide perovskite. *Nat. Nanotechnol.* **2014,** *9* (9), 687-692.

7.   Xu, W.; Hu, Q.; Bai, S.; Bao, C.; Miao, Y.; Yuan, Z.; Borzda, T.; Barker, A. J.; Tyukalova, E.; Hu, Z.; Kawecki, M.; Wang, H.; Yan, Z.; Liu, X.; Shi, X.; Uvdal, K.; Fahlman, M.; Zhang, W.; Duchamp, M.; Liu, J.-M.; Petrozza, A.; Wang, J.; Liu, L.-M.; Huang, W.; Gao, F., Rational molecular passivation for high-performance perovskite light-emitting diodes. *Nat. Photonics* **2019,** *13* (6), 418-424.

8.   Lin, K.; Xing, J.; Quan, L. N.; de Arquer, F. P. G.; Gong, X.; Lu, J.; Xie, L.; Zhao, W.; Zhang, D.; Yan, C.; Li, W.; Liu, X.; Lu, Y.; Kirman, J.; Sargent, E. H.; Xiong, Q.; Wei, Z., Perovskite light-emitting diodes with external quantum efficiency exceeding 20 per cent. *Nature* **2018,** *562* (7726), 245-248.

9.   Cao, Y.; Wang, N.; Tian, H.; Guo, J.; Wei, Y.; Chen, H.; Miao, Y.; Zou, W.; Pan, K.; He, Y.; Cao, H.; Ke, Y.; Xu, M.; Wang, Y.; Yang, M.; Du, K.; Fu, Z.; Kong, D.; Dai, D.; Jin, Y.; Li, G.; Li, H.; Peng, Q.; Wang, J.; Huang, W., Perovskite light-emitting diodes based on spontaneously formed submicrometre-scale structures. *Nature* **2018,** *562* (7726), 249-253.

10.   Chiba, T.; Hayashi, Y.; Ebe, H.; Hoshi, K.; Sato, J.; Sato, S.; Pu, Y.-J.; Ohisa, S.; Kido, J., Anion-exchange red perovskite quantum dots with ammonium iodine salts for highly efficient light-emitting devices. *Nat. Photonics* **2018,** *12* (11), 681-687.

11.   Wang, N.; Cheng, L.; Ge, R.; Zhang, S.; Miao, Y.; Zou, W.; Yi, C.; Sun, Y.; Cao, Y.; Yang, R.; Wei, Y.; Guo, Q.; Ke, Y.; Yu, M.; Jin, Y.; Liu, Y.; Ding, Q.; Di, D.; Yang, L.; Xing, G.; Tian, H.; Jin, C.; Gao, F.; Friend, R. H.; Wang, J.; Huang, W., Perovskite light-emitting diodes based on solution-processed self-organized multiple quantum wells. *Nat. Photonics* **2016,** *10* (11), 699-704.

12.   Ban, M.; Zou, Y.; Rivett, J. P. H.; Yang, Y.; Thomas, T. H.; Tan, Y.; Song, T.; Gao, X.; Credgington, D.; Deschler, F.; Sirringhaus, H.; Sun, B., Solution-processed perovskite light emitting diodes with efficiency exceeding 15% through additive-controlled nanostructure tailoring. *Nat. Commun.* **2018,** *9* (1), 3892.

13.   Stranks, S. D.; Hoye, R. L. Z.; Di, D.; Friend, R. H.; Deschler, F., The Physics of Light Emission in Halide Perovskite Devices. *Adv. Mater.* **2019***, 31*, 1803336.

14.   Shi, Y.; Wu, W.; Dong, H.; Li, G.; Xi, K.; Divitini, G.; Ran, C.; Yuan, F.; Zhang, M.; Jiao, B.; Hou, X.; Wu, Z., A Strategy for Architecture Design of Crystalline Perovskite Light-Emitting Diodes with High Performance. *Adv. Mater.* **2018,** *30* (25), 1800251.

15.   Fakharuddin, A.; Qiu, W.; Croes, G.; Devižis, A.; Gegevičius, R.; Vakhnin, A.; Rolin, C.; Genoe, J.; Gehlhaar, R.; Kadashchuk, A.; Gulbinas, V.; Heremans, P., Reduced Efficiency Roll-Off and Improved Stability of Mixed 2D/3D Perovskite Light Emitting Diodes by Balancing Charge Injection. *Adv. Funct. Mater.* **2019,** *29* (37), 1904101.

16.   Wang, J.; Song, C.; He, Z.; Mai, C.; Xie, G.; Mu, L.; Cun, Y.; Li, J.; Wang, J.; Peng, J.; Cao, Y., All-Solution-Processed Pure Formamidinium-Based Perovskite Light-Emitting Diodes. *Adv. Mater.* **2018,** *30* (39), 1804137.

17.   Kim, H.; Zhao, L.; Price, J. S.; Grede, A. J.; Roh, K.; Brigeman, A. N.; Lopez, M.; Rand, B. P.; Giebink, N. C., Hybrid perovskite light emitting diodes under intense electrical excitation. *Nat. Commun.* **2018,** *9* (1), 4893.

18. Liu, B.; Wang, L.; Gu, H.; Sun, H.; Demir, H. V., Highly Efficient Green Light-Emitting Diodes from All-Inorganic Perovskite Nanocrystals Enabled by a New Electron Transport Layer. *Adv. Opt. Mater.* **2018,** *6* (11), 1800220.

19. Li, J.; Xu, L.; Wang, T.; Song, J.; Chen, J.; Xue, J.; Dong, Y.; Cai, B.; Shan, Q.; Han, B.; Zeng, H., 50-Fold EQE Improvement up to 6.27% of Solution-Processed All-Inorganic Perovskite $CsPbBr_3$ QLEDs via Surface Ligand Density Control. *Adv. Mater.* **2017,** *29* (5), 1603885.

20. Wang, J.; Wang, N.; Jin, Y.; Si, J.; Tan, Z.-K.; Du, H.; Cheng, L.; Dai, X.; Bai, S.; He, H.; Ye, Z.; Lai, M. L.; Friend, R. H.; Huang, W., Interfacial Control Toward Efficient and Low-Voltage Perovskite Light-Emitting Diodes. *Adv. Mater.* **2015,** *27* (14), 2311-2316.

21. Sun, Z.; Ding, B.; Wu, B.; You, Y.; Ding, X.; Hou, X., LiF Layer at the Interface of Au Cathode in Organic Light-Emitting Devices: A Nonchemical Induced Carrier Injection Enhancement. *J. Phys. Chem. C* **2012,** *116* (3), 2543-2547.

22. Jabbour, G. E.; Kawabe, Y.; Shaheen, S. E.; Wang, J. F.; Morrell, M. M.; Kippelen, B.; Peyghambarian, N., Highly efficient and bright organic electroluminescent devices with an aluminum cathode. *Appl. Phys. Lett.* **1997,** *71* (13), 1762-1764.

23. Hung, L. S.; Tang, C. W.; Mason, M. G., Enhanced electron injection in organic electroluminescence devices using an Al/LiF electrode. *Appl. Phys. Lett.* **1997,** *70* (2), 152-154.

24. Schmitz, C.; Schmidt, H.-W.; Thelakkat, M., Lithium−Quinolate Complexes as Emitter and Interface Materials in Organic Light-Emitting Diodes. *Chem. Mater.* **2000,** *12* (10), 3012-3019.

25. Huang, J.; Li, G.; Wu, E.; Xu, Q.; Yang, Y., Achieving High-Efficiency Polymer White-Light-Emitting Devices. *Adv. Mater.* **2006,** *18* (1), 114-117.

26. Jabbour, G. E.; Kippelen, B.; Armstrong, N. R.; Peyghambarian, N., Aluminum based cathode structure for enhanced electron injection in electroluminescent organic devices. *Appl. Phys. Lett.* **1998,** *73* (9), 1185-1187.

27. Yang, X.; Mo, Y.; Yang, W.; Yu, G.; Cao, Y., Efficient polymer light emitting diodes with metal fluoride/Al cathodes. *Appl. Phys. Lett.* **2001,** *79* (5), 563-565.

28. Chin, X. Y.; Perumal, A.; Bruno, A.; Yantara, N.; Veldhuis, S. A.; Martínez-Sarti, L.; Chandran, B.; Chirvony, V.; Lo, A. S.-Z.; So, J.; Soci, C.; Grätzel, M.; Bolink, H. J.; Mathews, N.; Mhaisalkar, S. G., Self-assembled hierarchical nanostructured perovskites enable highly efficient LEDs via an energy cascade. *Energy Environ. Sci.* **2018,** *11* (7), 1770-1778.

29. Yantara, N.; Bhaumik, S.; Yan, F.; Sabba, D.; Dewi, H. A.; Mathews, N.; Boix, P. P.; Demir, H. V.; Mhaisalkar, S., Inorganic Halide Perovskites for Efficient Light-Emitting Diodes. *J. Phys. Chem. Lett.* **2015,** *6* (21), 4360-4364..

30. Chiba, T.; Hoshi, K.; Pu, Y.-J.; Takeda, Y.; Hayashi, Y.; Ohisa, S.; Kawata, S.; Kido, J., High-Efficiency Perovskite Quantum-Dot Light-Emitting Devices by Effective Washing Process and Interfacial Energy Level Alignment. *ACS Appl. Mater. Interfaces* **2017,** *9* (21), 18054-18060.

31. Angel, F. A.; Gao, R.; Wallace, J. U.; Tang, C. W., Silver-induced activation of 8-hydroxyquinolinato lithium as electron injection material in single-stack and tandem OLED devices. *Org. Electron.* **2018,** *59*, 220-223.

32. Sun, X.; Zhou, D.-Y.; Qiu, L.; Liao, L.-S.; Yan, F., Sodium−Quinolate Complexes as Efficient Electron Injection Materials for Organic Light-Emitting Diode Devices. *J. Phys. Chem. C* **2011,** *115* (5), 2433-2438.

33. Xie, K.; Qiao, J.; Duan, L.; Li, Y.; Zhang, D.; Dong, G.; Wang, L.; Qiu, Y., Organic cesium salt as an efficient electron injection material for organic light-emitting diodes. *Appl. Phys. Lett.* **2008,** *93* (18), 183302.

34. Lee, Y. M.; Park, Y.; Yi, Y.; Kim, J. W., Deposition sequence dependent variation in interfacial chemical reactions between 8-hydroxyquinolatolithium and Al. *Appl. Phys. Lett.* **2008,** *93* (12), 123301.

35. Siemund, H.; Göbel, H., Numerical Simulation of Organic Light-Emitting Diodes With Insulating Cathode Buffer Layer. *IEEE Trans. Electron Devices* **2016,** *63* (9), 3700-3706.

36. Kim, Y., Power-law-type electron injection through lithium fluoride nanolayers in phosphorescence organic light-emitting devices. *Nanotechnology* **2008,** *19* (35), 355207.

37. Heeger, A. J.; Parker, I. D.; Yang, Y., Carrier injection into semiconducting polymers: Fowler-Nordheim field-emission tunneling. *Synth. Met.* **1994,** *67* (1), 23-29.

38.   Quintero-Bermudez, R.; Kirman, J.; Ma, D.; Sargent, E. H.; Quintero-Torres, R., Mechanisms of LiF Interlayer Enhancements of Perovskite Light-Emitting Diodes. *J. Phys. Chem. Lett.* **2020**, 11 (10), 4213-4220.

39.   Brown, T. M.; Friend, R. H.; Millard, I. S.; Lacey, D. J.; Burroughes, J. H.; Cacialli, F., LiF/Al cathodes and the effect of LiF thickness on the device characteristics and built-in potential of polymer light-emitting diodes. *Appl. Phys. Lett.* **2000,** *77* (19), 3096-3098.

40.   Zheng, X.; Wu, Y.; Sun, R.; Zhu, W.; Jiang, X.; Zhang, Z.; Xu, S., Efficiency improvement of organic light-emitting diodes using 8-hydroxy-quinolinato lithium as an electron injection layer. *Thin Solid Films* **2005,** *478* (1), 252-255.

41.   Hassanabadi, E.; Latifi, M.; Gualdrón-Reyes, A. F.; Masi, S.; Yoon, S. J.; Poyatos, M.; Julian-Lopez, B.; Mora-Seró, I., Ligand & Band Gap Engineering: Tailoring the Protocol Synthesis for Achieving High-Quality CsPbI3 Quantum Dots. *Nanoscale*, **2020**, DOI: 10.1039/D0NR03180A.

42.   Zolfaghari, Z.; Hassanabadi, E.; Pitarch-Tena, D.; Yoon, S. J.; Shariatinia, Z.; van de Lagemaat, J.; Luther, J. M.; Mora-Seró, I., Operation Mechanism of Perovskite Quantum Dot Solar Cells Probed by Impedance Spectroscopy. *ACS Energy Lett.* **2019,** *4* (1), 251-258.

43.   Protesescu, L.; Yakunin, S.; Bodnarchuk, M. I.; Krieg, F.; Caputo, R.; Hendon, C. H.; Yang, R. X.; Walsh, A.; Kovalenko, M. V., Nanocrystals of Cesium Lead Halide Perovskites ($CsPbX_3$, X = Cl, Br, and I): Novel Optoelectronic Materials Showing Bright Emission with Wide Color Gamut. *Nano Lett.* **2015,** *15* (6), 3692-3696.

44.   Swarnkar, A.; Marshall, A. R.; Sanehira, E. M.; Chernomordik, B. D.; Moore, D. T.; Christians, J. A.; Chakrabarti, T.; Luther, J. M., Quantum dot–induced phase stabilization of α-$CsPbI_3$ perovskite for high-efficiency photovoltaics. *Science* **2016,** *354* (6308), 92-95.

45.   Liu, F.; Zhang, Y.; Ding, C.; Kobayashi, S.; Izuishi, T.; Nakazawa, N.; Toyoda, T.; Ohta, T.; Hayase, S.; Minemoto, T.; Yoshino, K.; Dai, S.; Shen, Q., Highly Luminescent Phase-Stable $CsPbI_3$ Perovskite Quantum Dots Achieving Near 100% Absolute Photoluminescence Quantum Yield. *ACS Nano* **2017,** *11* (10), 10373-10383.

46.   Krieg, F.; Ochsenbein, S. T.; Yakunin, S.; ten Brinck, S.; Aellen, P.; Süess, A.; Clerc, B.; Guggisberg, D.; Nazarenko, O.; Shynkarenko, Y.; Kumar, S.; Shih, C.-J.; Infante, I.; Kovalenko, M. V., Colloidal $CsPbX_3$ (X = Cl, Br, I) Nanocrystals 2.0: Zwitterionic Capping Ligands for Improved Durability and Stability. *ACS Energy Lett.* **2018,** *3* (3), 641-646.

47.   Tan, Y.; Zou, Y.; Wu, L.; Huang, Q.; Yang, D.; Chen, M.; Ban, M.; Wu, C.; Wu, T.; Bai, S.; Song, T.; Zhang, Q.; Sun, B., Highly Luminescent and Stable Perovskite Nanocrystals with Octylphosphonic Acid as a Ligand for Efficient Light-Emitting Diodes. *ACS Appl. Mater. Interfaces* **2018,** *10* (4), 3784-3792.

48.   Song, C.; Zhong, Z.; Hu, Z.; Wang, J.; Wang, L.; Ying, L.; Wang, J.; Cao, Y., Methanol treatment on low-conductive PEDOT:PSS to enhance the PLED's performance. *Org. Electron.* **2016,** *28*, 252-256.

49.   Sanehira, E. M.; Marshall, A. R.; Christians, J. A.; Harvey, S. P.; Ciesielski, P. N.; Wheeler, L. M.; Schulz, P.; Lin, L. Y.; Beard, M. C.; Luther, J. M., Enhanced mobility $CsPbI_3$ quantum dot arrays for record-efficiency, high-voltage photovoltaic cells. *Sci. Adv.* **2017,** *3* (10), eaao4204.